DEVELOPMENTAL NEUROSCIENCE

Deterministic splicing of *Dscam2* is regulated by Muscleblind

Joshua Shing Shun Li and S. Sean Millard*

Alternative splicing increases the proteome diversity crucial for establishing the complex circuitry between trillions of neurons. To provide individual cells with different repertoires of protein isoforms, however, this process must be regulated. Previously, we found that the mutually exclusive alternative splicing of *Drosophila Dscam2* produces two isoforms (A and B) with unique binding properties. This splicing event is cell type specific, and the transmembrane proteins that it generates are crucial for the development of axons, dendrites, and synapses. Here, we show that Muscleblind (Mbl) controls *Dscam2* alternative splicing. Mbl represses isoform A and promotes the selection of isoform B. *Mbl* mutants exhibit phenotypes also observed in flies engineered to express a single *Dscam2* isoform. Consistent with this, *mbl* expression is cell type specific and correlates with the splicing of isoform B. Our study demonstrates how the regulated expression of a splicing factor is sufficient to provide neurons with unique protein isoforms crucial for development.

INTRODUCTION

Alternative splicing occurs in approximately 95% of human genes and generates proteome diversity much needed for brain wiring (*1*, *2*). Specifying neuronal connections through alternative splicing would require regulated expression of isoforms with unique functions in different cell types to carry out distinct processes. Although there are some examples of neuronal cell type–specific isoform expression (*3*–*8*), the mechanisms underlying these deterministic splicing events and their functional consequences remain understudied. This is due, in part, to the technical difficulties of assessing and manipulating isoform expression in vivo and at the single-cell level. Another obstacle is that most splicing regulators are proposed to be ubiquitously expressed (*9*). For example, the broadly expressed SR and heterogeneous nuclear ribonucleoproteins typically have opposing activities, and the prevalence of splice site usage is thought to be controlled by their relative abundances within the cell (*10*). Although there are many examples where splicing regulators are expressed in a tissue-specific manner (*11*–*16*), until recently, reports of cell type–specific expression have been less frequent (*17*, *18*).

In insects, Dscam2 is a cell recognition molecule that mediates self- and cell type–specific avoidance (tiling) (*19*–*21*). Mutually exclusive alternative splicing of exon 10A or 10B produces two isoforms with biochemically unique extracellular domains that are regulated both spatially and temporally (*19*, *21*). Previously, we demonstrated that cell type–specific alternative splicing of *Drosophila Dscam2* is crucial for the proper development of axon terminal size, dendrite morphology, and synaptic numbers in the fly visual system (*4*, *22*, *23*). Although these studies showed that disrupting cell-specific *Dscam2* alternative splicing has functional consequences, what regulates this process remained unclear. Here, we conducted an RNA interference (RNAi) screen and identified *muscleblind* (*mbl*) as a regulator of *Dscam2* alternative splicing. Loss-of-function (LOF) and overexpression (OE) studies suggest that Mbl acts both as a splicing repressor of *Dscam2* exon 10A and as an activator of exon 10B (hereafter *Dscam2.10A* and *Dscam2.10B*). Consistent with this finding, *mbl* expression is cell type specific and correlates with the expression of *Dscam2.10B*. Hypomorphic *mbl* mutants exhibit visual system phenotypes that are similar to those observed in flies engineered to express one isoform in all *Dscam2*-positive cells (single-isoform strains). Similarly, driving *mbl* in mushroom body (MB) neurons that normally select isoform A induces the expression of isoform B and generates a single-isoform phenotype. Although the *mbl* gene is itself alternatively spliced, we found that selection of *Dscam2.10B* does not require a specific Mbl isoform and that human MBNL1 can also regulate *Dscam2* alternative splicing. Our study provides compelling genetic evidence that the regulated expression of a highly conserved RNA binding protein, Mbl, is sufficient for the selection of *Dscam2.10B* and that disrupting this mechanism for cell-specific protein expression leads to developmental defects in neurons.

RESULTS

An RNAi screen identifies *mbl* as a repressor of *Dscam2* exon 10A selection

We reasoned that the neuronal cell type–specific alternative splicing of *Dscam2* is likely regulated by RNA binding proteins and that we could identify these regulators by knocking them down in a genetic background containing an isoform reporter. In photoreceptors (R cells) of third-instar larvae, *Dscam2.10B* is selected, whereas the splicing of *Dscam2.10A* is repressed (*4*, *24*). Given that quantifying a reduction in *Dscam2.10B* isoform reporter levels is challenging compared to detecting the appearance of *Dscam2.10A* in cells where it is not normally expressed, we performed a screen for repressors of isoform A in R cells.

To knock down RNA binding proteins, the *glass* multimer reporter *(GMR)-GAL4* was used to drive RNAi transgenes selectively in R cells. Our genetic background included *UAS-Dcr-2* to increase RNAi efficiency and *GMR-GFP* to mark the photoreceptors independent of the *Gal4/UAS* system (*25*). Last, a *Dscam2.10A-LexA* reporter driving *LexAOp*-myristolated tdTomato (hereafter *Dscam2.10A>tdTom*; Fig. 1A) was used to visualize isoform A expression (*24*). As expected, *Dscam2.10B>tdTom* was detected in R cell projections in the lamina plexus as well as in their cell bodies in the eye disc, whereas *Dscam2.10A>tdTom* was not (Fig. 1, C and D). OE of Dcr-2 in R cells did not perturb the repression of *Dscam2.10A* (Fig. 1O).

School of Biomedical Sciences, Faculty of Medicine, The University of Queensland, Brisbane, Queensland 4072, Australia.
*Corresponding author. Email: s.millard@uq.edu.au

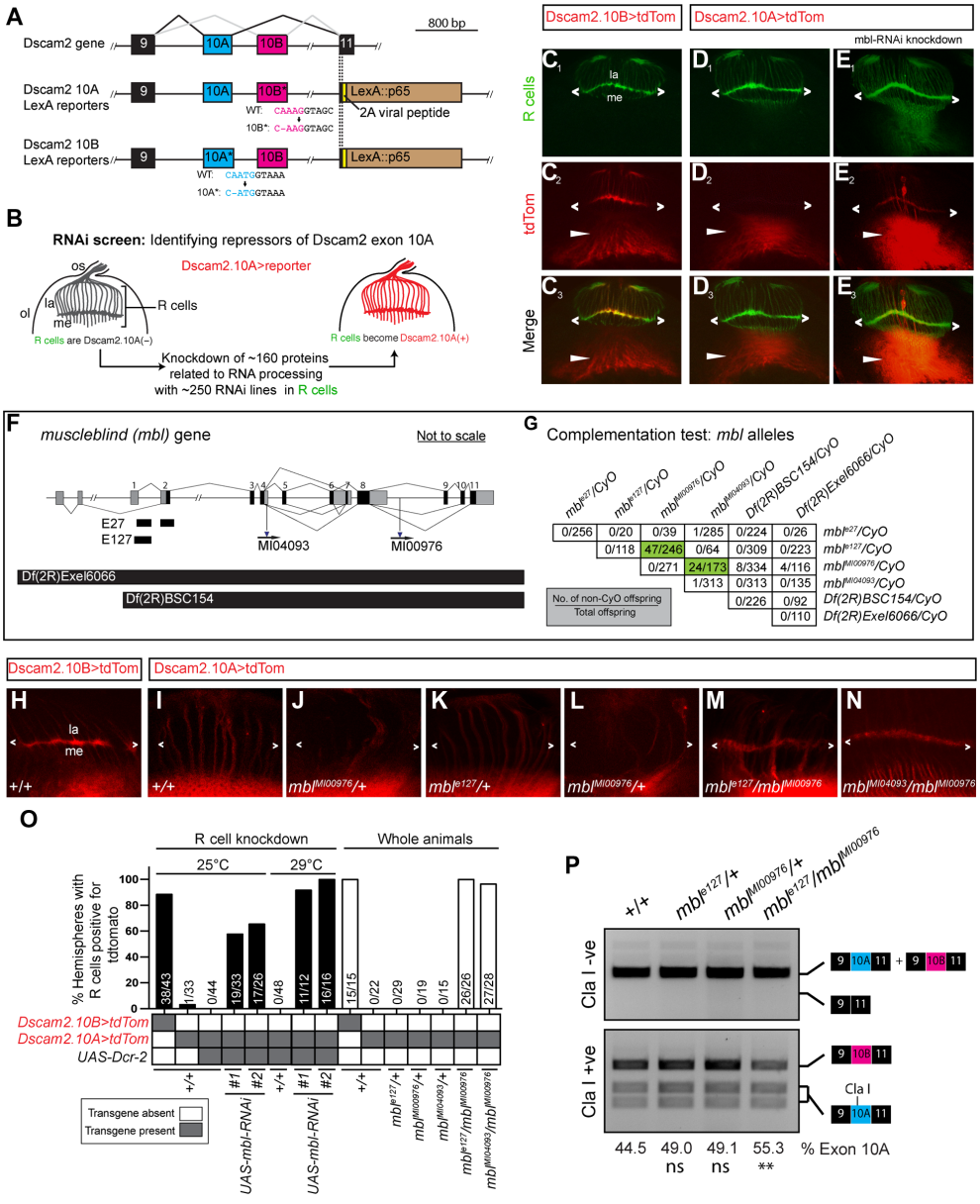

Fig. 1. *Drosophila mbl* is required for the repression of *Dscam2* exon 10A in R cells. (**A**) Schematic showing the region of *Dscam2* exon 10 that undergoes mutually exclusive alternative splicing and the *LexA* isoform-specific reporter lines. Frameshift mutations in the exon not reported are shown. WT, wild-type. (**B**) Schematic RNAi screen design for identifying repressors of *Dscam2* exon 10A selection. R cells normally select exon 10B and repress exon 10A. We knocked down RNA binding proteins in R cells while monitoring 10A expression. os, optic stalk; ol, optic lobe; la, lamina; me, medulla. (**C** to **E**) *Dscam2* exon 10A is derepressed in R cells when *mbl* is knocked down. (C_1 to C_3) *Dscam2.10B* control. R cells (green) normally select exon 10B (red). R cell terminals can be observed in the lamina plexus (angle brackets). *Dscam2.10B* is also expressed in the developing optic lobe (arrowheads). (D_1 to D_3) *Dscam2.10A* is not expressed in R cells (green) but is expressed in the developing optic lobe (arrowheads). (E_1 to E_3) RNAi lines targeting *mbl* in R cells result in the aberrant expression of *Dscam2.10A* in R cells. (**F**) Schematic of the *mbl* gene showing the location of two small deletions (*E27* and *E127*), two MiMIC insertions (*MI04093* and *MI00976*), and two deficiencies [*Df(2R)Exel6066* and *Df(2R)BSC154*] used in this study. Noncoding exons are in gray, and coding exons are black. (**G**) Complementation test of *mbl* LOF alleles. Numbers in the table represent the number of non-*CyO* offspring over the total. Most transheterozygote combinations were lethal with the exception of $mbl^{MI00976}/mbl^{e27}$ and $mbl^{MI00976}/mbl^{MI04093}$ (green). (**H** to **N**) *Mbl* transheterozygotes express *Dscam2.10A* in R cells. (H) *Dscam2.10B* control showing expression in the lamina plexus (angle brackets). (I) *Dscam2.10A* control showing no expression of this isoform in R cells. (J to L) Heterozygous animals for *mbl* LOF alleles are comparable to control. (M and N) Two different *mbl* transheterozygote combinations exhibit derepression of *Dscam2.10A* in R cells. (**O**) Quantification of *Dscam2.10>tdTom* expression in third-instar R cells with various *mbl* manipulations, including RNAi knockdown (black bars) and whole-animal transheterozygotes (white bars). *Y* axis represents the number of optic lobes, with R cells positive for tdTom over total quantified as a percentage. On the *x* axis, the presence of a transgene is indicated with a gray box, and the temperature at which the crosses were reared (25° or 29°C) is indicated on the top. (**P**) *Dscam2* exon 10A inclusion is increased in *mbl* transheterozygotes. Top: Semiquantitative RT-PCR from different genotypes indicated. Primers amplified the variable region that includes exon 10. A smaller product that would result from exon 10 skipping is not observed. Bottom: Exon 10A–specific cleavage with restriction enzyme Cla I shows an increase in exon 10A inclusion in *mbl* transheterozygotes. The percentage of exon 10A inclusion was calculated by dividing 10A by 10A+10B bands following restriction digest. The mean of exon 10A inclusion is shown at the bottom of each lane. Analysis of variance (ANOVA) test with Tukey's multiple comparison test was used to compare the exon 10A inclusion. ns, $P > 0.05$; $^{**}P < 0.01$. See also figs. S1 and S2.

We knocked down ~160 genes using ~250 RNAi lines (Fig. 1B and table S1) and identified two independent RNAi lines targeting *mbl* that caused aberrant expression of *Dscam2.10A* in R cells where it is normally absent (Fig. 1, F and O). The penetrance increased when animals were reared at a more optimal Gal4 temperature of 29°C (Fig. 1O) (*26*).

Mbl family proteins have evolutionarily conserved tandem CCCH zinc-finger domains through which they bind pre-mRNA. Vertebrate Mbl family members are involved in tissue-specific splicing and have been implicated in myotonic dystrophy (*27*). Formerly known as *mindmelt*, *Drosophila mbl* was first identified in a second chromosome *P*-element genetic screen for embryonic defects in the peripheral nervous system (*28*). *Mbl* produces multiple isoforms through alternative splicing (*29*, *30*), and its function has been most extensively characterized in fly muscles, where both hypomorphic mutations and sequestration of the protein by repeated *CUG* sequences within an mRNA lead to muscle defects (*31*). To validate the RNAi phenotype, we tested *Dscam2.10A>tdTom* expression in *mbl* LOF mutants. Because *mbl* LOF results in lethality, we first conducted complementation tests on six *mbl* mutant alleles to identify viable hypomorphic combinations. These included two alleles created previously via imprecise *P*-element excision (mbl^{e127} and mbl^{e27}), two MiMIC (Minos Mediated Integration Cassette) splicing traps ($mbl^{MI00976}$ and $mbl^{MI04093}$), and two second chromosome deficiencies [*Df(2R)BSC154* and *Df(2R)Exel6066*] (Fig. 1, F and G). Consistent with previous reports, the complementation tests confirmed that the majority of the alleles were lethal over one another (Fig. 1G) (*28*). However, we identified two *mbl* transheterozygous combinations that were partially viable and crossed these into a *Dscam2.10A>tdTom* reporter background. Both $mbl^{e127}/mbl^{MI00976}$ and $mbl^{MI04093}/mbl^{MI00976}$ animals presented aberrant *Dscam2.10A* expression in R cells when compared to heterozygous and wild-type controls (Fig. 1, H to O). *Mbl* mutant mosaic clones also exhibited aberrant *Dscam2.10A>tdTom* expression in R cells (fig. S1, A to F). The weakest allele, mbl^{M00976}, which removes only a proportion of the *mbl* isoforms, was the only exception (fig. S1, E and F).

One alternative explanation of how *Dscam2.10A>tdTom* expression could get switched on in *mbl* mutants is through exon 10 skipping. Removing both alternative exons simultaneously does not result in a frameshift mutation, and because the Gal4 in our reporters is inserted directly downstream of the variable exons (in exon 11), it would still be expressed. To test this possibility, we amplified *Dscam2* sequences between exons 9 and 11 in $mbl^{e127}/mbl^{MI00976}$ transheterozygous animals using reverse transcription polymerase chain reaction (RT-PCR). In both control and *mbl* LOF mutants, we detected RT-PCR products [~690 base pairs (bp)] that corresponded to the inclusion of exon 10 (A or B) and failed to detect products (~390 bp) that would result from exon 10 skipping (Fig. 1P). This suggested that Mbl is not involved in the splicing fidelity of *Dscam2.10* but rather in the selective mutual exclusion of its two isoforms. To assess whether the ratios of the two isoforms were changing in the *mbl* hypomorphic mutants, we cut the exon 10 RT-PCR products with the Cla I restriction enzyme that only recognizes exon 10A. Densitometric analysis then allowed us to semiquantitatively compare the relative levels of both isoforms. There was a ~25% increase in the level of exon 10A inclusion in $mbl^{e127}/mbl^{MI00976}$ animals compared to controls (Fig. 1P). Similarly, quantitative RT-PCR (qRT-PCR) of the $mbl^{e127}/mbl^{MI00976}$ animals showed a ~1.25- and ~0.78-fold change in exon 10A and 10B inclusion, respectively, when compared to controls. Both results are consistent with the derepression that we observed in our 10A reporter lines. To determine whether Mbl was specifically regulating *Dscam2* exon 10 mutually exclusive splicing, we assessed other *Dscam2* alternative splicing events. These included an alternative 5′ splice site selection of *Dscam2* exon 19 and the alternative last exon selection of exon 20 (fig. S2A). The expression of these different isoforms was unchanged in *mbl* hypomorphic mutants (fig. S2B). Together, our results indicate that Mbl is an essential splicing factor that specifically represses *Dscam2.10A*.

Mbl is necessary for the selection of *Dscam2* exon 10B

Because *Dscam2* exon 10 isoforms are mutually exclusively spliced, we predicted that selection of exon 10A would lead to the loss of exon 10B selection. To test this, we conducted mosaic analysis with a repressible cell marker (MARCM) (*32*) to analyze *Dscam2.10B* expression in *mbl* mutant clones. In late third-instar brains, clones homozygous [green fluorescent protein (GFP) positive] for mbl^{e127} and mbl^{e27} exhibited a marked reduction in *Dscam2.10B>tdTom* expression in R cell axons projecting to the lamina plexus compared to controls (Fig. 2, B, C, and E). The absence of *Dscam2.10B>tdTom* in *mbl* mutant clones was more notable during pupal stages (Fig. 2D), suggesting that perdurance of Mbl could explain the residual signal observed in third-instar animals. These results reveal that *mbl* is cell-autonomously required for the selection of *Dscam2.10B*.

Mbl expression is cell type specific and correlates with *Dscam2.10B* selection

Previous studies have reported that *mbl* is expressed in third-instar eye discs and muscles (*31*, *33*). Because *mbl* LOF results in both the selection of *Dscam2.10A* and the loss of *Dscam2.10B*, we predicted that *mbl* expression would correlate with the presence of isoform B. To test this, we characterized several *mbl* reporters (fig. S3A). We analyzed three enhancer trap strains (transcriptional reporters) inserted near the beginning of the *mbl* gene (mbl^{k01212}-*LacZ*, mbl^{NP1161}-*Gal4*, and mbl^{NP0420}-*Gal4*), as well as a splicing trap line generated by the Trojan-mediated conversion of an *mbl* MiMIC insertion (fig. S2A, $mbl^{MiMIC00139}$-*Gal4*) (*34*). The splicing trap reporter consists of a splice acceptor site and an in-frame *T2A-Gal4* sequence inserted in an intron between two coding exons. This *Gal4* cassette gets incorporated into *mbl* mRNA during splicing, and therefore, Gal4 is only present when *mbl* is translated. Consistent with previous studies, and its role in repressing the production of *Dscam2.10A*, all four *mbl* reporters were expressed in the third-instar photoreceptors (Fig. 3A and fig. S3, A to D). We next did a more extensive characterization of *mbl* expression by driving nuclear localized GFP (*GFP.nls*) with one transcriptional (mbl^{NP0420}-*Gal4*) and one translational ($mbl^{MiMIC00139}$-*Gal4*) reporter. In the brain, we found that *mbl* was expressed predominantly in postmitotic neurons, with some expression detected in glial cells (fig. S3, C to H and J to M). We detected the translational, but not the transcriptional, reporter in third-instar muscles (fig. S3, I and N). The absence of expression is likely due to the insertion of the *P*-element into a neural-specific enhancer, as previously described (*35*). To assess the expression of *mbl* in the five lamina neurons, L1 to L5, all of which express *Dscam2* (*4*, *24*), we implemented an intersectional strategy using a *UAS>stop>epitope* reporter (*36*) that is dependent on both *FLP* and *Gal4*. The *FLP* source (*Dac-FLP*) was expressed in lamina neurons and was able to remove the transcriptional stop motif in the reporter transgene. The overlap between *mbl-Gal4* and *Dac-FLP* allowed us

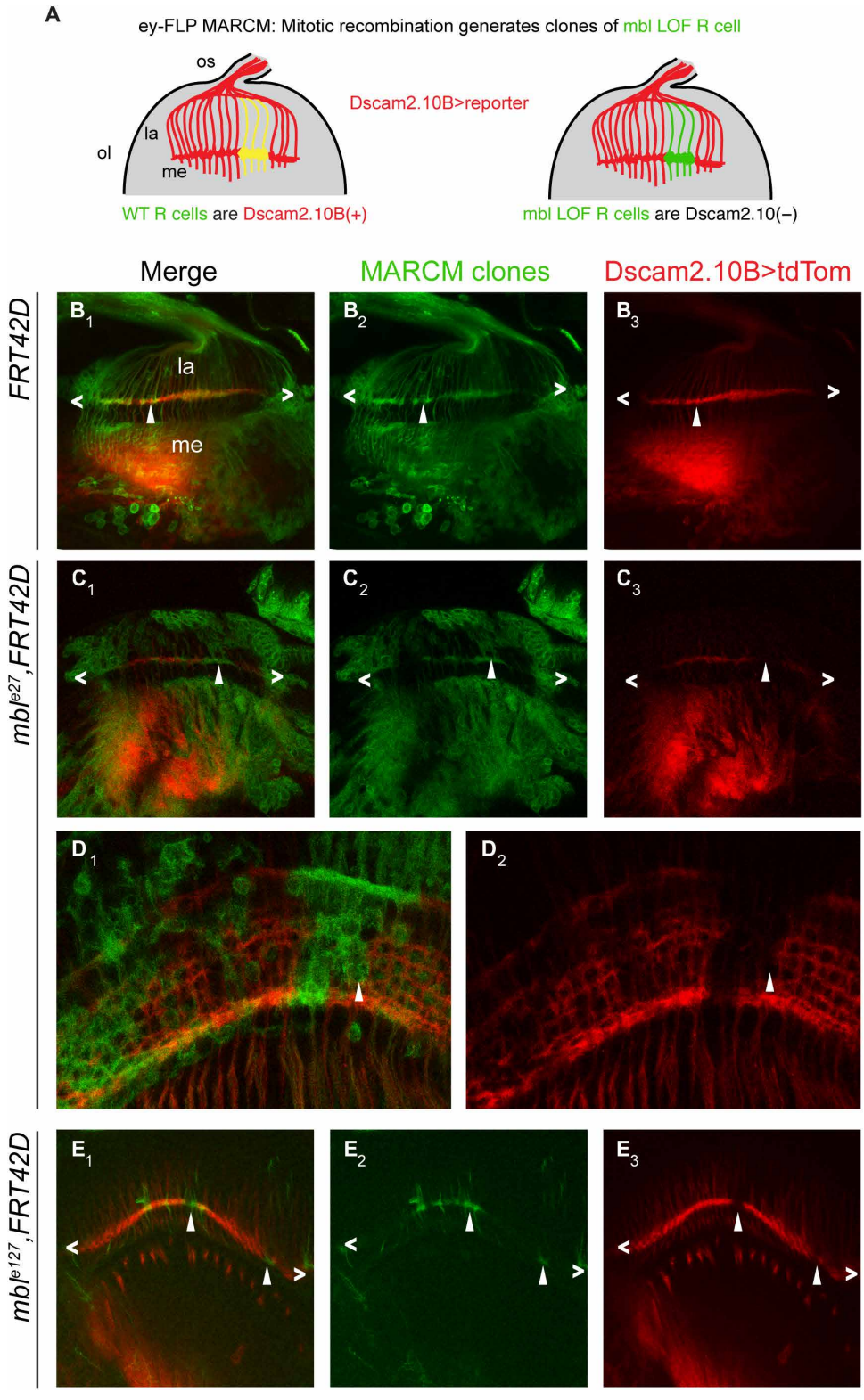

Fig. 2. *Drosophila mbl* is necessary for the selection of *Dscam2* exon 10B in R cells. (**A**) Schematic of our predicted *mbl* MARCM results using *ey-FLP*. Wild-type R cell clones will be GFP(+) and *Dscam2.10B>tdTom*(+) (yellow), whereas *mbl* mutant clones will be *Dscam2.10B>tdTom*(−) (green). (**B_1** to **B_3**) Control MARCM clones (green) in third-instar R cells (angle brackets) are positive for *Dscam2.10B>tdTom* (arrowheads). (**C_1** to **C_3**) In *mbl*^{e27} clones, *Dscam2.10B* labeling in the lamina plexus is discontinuous, and its absence correlates with the loss of *mbl* (arrowheads). (**D_1** and **D_2**) *Mbl* MARCM clones from midpupal optic lobes lack *Dscam2.10B*>tdTom. (**E_1** to **E_3**) A different allele (*mbl*^{e127}) exhibits a similar phenotype in third-instar brains.

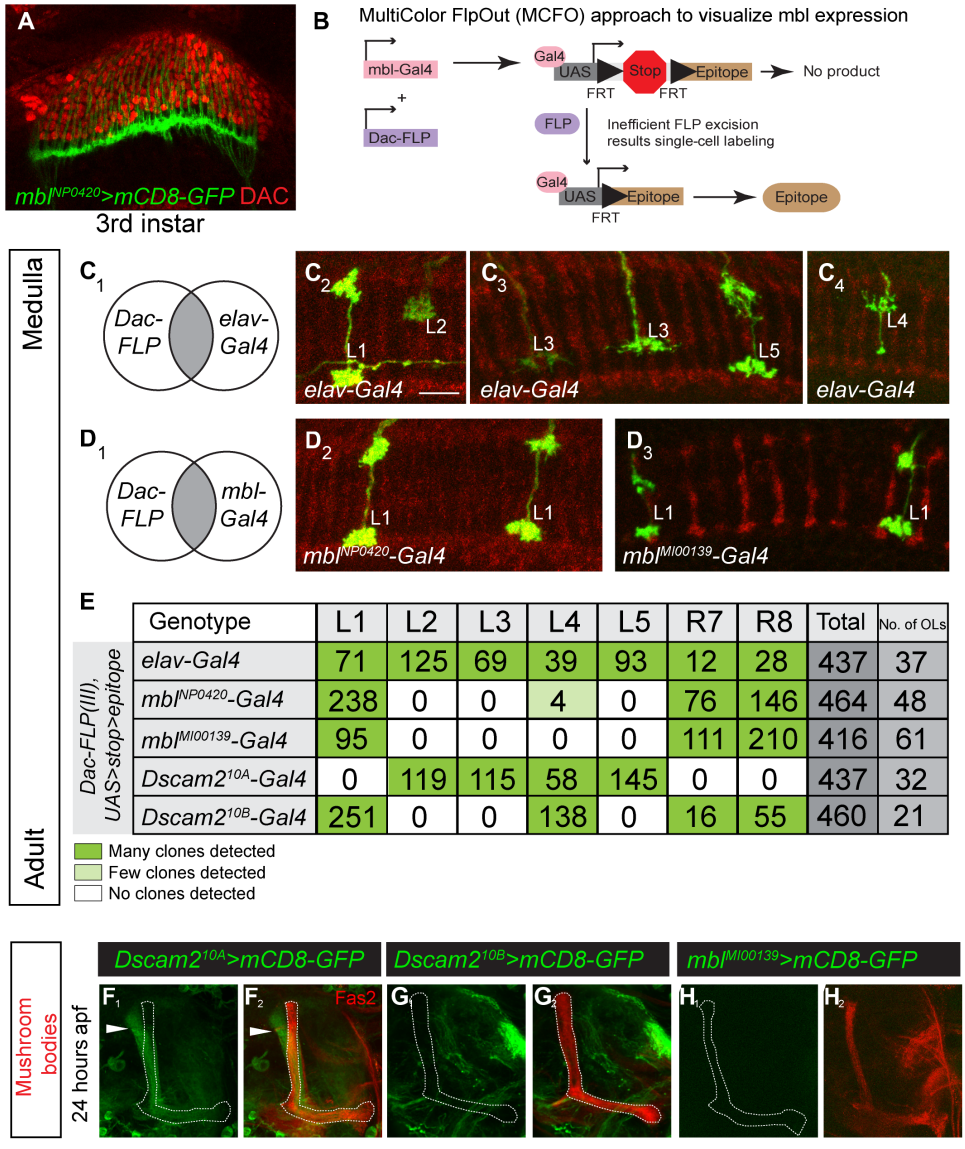

Fig. 3. *Mbl* is expressed in a cell-specific manner that correlates with *Dscam2.10B*. (**A**) An *mbl-Gal4* reporter (green) is expressed in third-instar R cells but not in lamina neuron precursor cells labeled with an antibody against Dacshund (DAC; red). (**B**) Schematic of MultiColor FlpOut (MCFO) approach to characterize *mbl* reporter expression in lamina neurons at adult stages. The *UAS FlpOut* construct produces an epitope-tagged version of a nonfluorescent GFP [smGFP (*36*)]. (**C_1** to **C_4**) All lamina neurons can be detected using an MCFO strategy with a pan-neuronal reporter (*elav-Gal4*). Lamina neurons were identified on the basis of their unique axon morphologies. (**D_1** to **D_4**) An intersectional strategy using *mbl-Gal4* primarily labels L1 lamina neurons. (**E**) Quantification of lamina neurons and R7 and R8 neurons observed using the intersectional strategy. Dark green and light green boxes represent high and low numbers of labeled neurons, respectively. (**F** to **H**) *Mbl* is not expressed in MB neurons that express *Dscam2.10A* at 24 hours apf. (F_1 and F_2) *Dscam2.10A* is expressed in α′β′ MB neurons that are not labeled by Fas2. Fas2 labels the αβ and γ subsets of MB neurons. (G and H) Neither *Dscam2.10B* (G_1 and G_2) nor *mbl* (H_1 and H_2) is detected in MB neurons. See also figs. S3 and S4.

to visualize *mbl* expression in lamina neurons at single-cell resolution (Fig. 3B). As a proof of principle, we first did an intersectional analysis with a pan-neuronal reporter, *elav-Gal4* (Fig. 3C_1). We detected many clones encompassing various neuronal cell types including the axons of L1 to L5 and R7 and R8 (Fig. 3, C and D). This confirmed that all lamina neurons could be detected using this strategy. Using *mbl-Gal4* reporters, we found that L1, R7, and R8, which expresses *Dscam2.10B*, were the primary neurons labeled. A few L4 cells were also detected, which is consistent with this neuron expressing *Dscam2.10B* early in development and *Dscam2.10A* at later stages (*24*). To confirm this finding, we dissected the expression of *mbl* in lamina neurons during development. Using the same intersectional strategy, we detected a high number of L4 clones at 48 hours after puparium formation (apf) (30%, $n = 10$). This was followed by a decline at 60 hours apf (26.7%, $n = 30$) and 72 hours apf (11.8%, $n = 85$), reaching the lowest at eclosion (fig. S4, A and B; 1.7%, $n = 242$). Thus, *mbl* expression in L4 neurons mirrors the expression of *Dscam2.10B*. Consistent with this, L2, L3, and L5 were all detected using the intersectional strategy with *Dscam2.10A-Gal4* but were not labeled using *mbl-Gal4* (Fig. 3E). Our intersectional *mbl* expression data are further strengthened by an independent RNA-sequencing study of isolated lamina neurons during development,

where *mbl* is detected at high levels in L1, R7, and R8 neurons (~5- to 100-fold more than L2 to L5) (*37*). Together, these results show that *mbl* expression correlates with the cell type–specific alternative splicing of *Dscam2.10B*. This suggests that the presence or absence of *mbl* can determine the selection of the *Dscam2.10* isoform in a cell.

Ectopic expression of multiple *mbl* isoforms is sufficient to promote the selection of *Dscam2* exon 10B

Because cells that select *Dscam2.10B* express *mbl* and cells that select *Dscam2.10A* lack *mbl*, we wondered whether it was sufficient to promote exon 10B selection in *Dscam2.10A*-positive cells. To test this, we ectopically expressed *mbl* with a ubiquitous driver (*Act5c-Gal4*) and monitored isoform B expression using *Dscam2.10B>tdTom*. We focused on the MB, as this tissue expresses isoform A specifically in α′β′ neurons at 24 hours apf where *mbl* is not detected (Figs. 3, G and H, 4, A to C). Consistent with our prediction, ectopic expression of *mbl* using an enhancer trap containing a *UAS* insertion at the 5′ end of the gene (*Act5c>mbl*$^{B2\text{-}E1}$) switched on *Dscam2.10B* in α′β′ MB neurons, where it is normally absent (Fig. 4D). Driving *mbl* with an MB-specific *Gal4* (*OK107*) gave similar results (Fig. 4E). Although our two *Gal4* drivers expressed *mbl* in all MB neurons, *Dscam2.10B* was only observed in α′β′ neurons, demonstrating that transcription of *Dscam2* is a prerequisite for this splicing modulation. Previous studies have suggested that the *mbl* gene is capable of generating different isoforms with unique functions depending on their subcellular localization (*38*). This also includes the production of a highly abundant circular RNA (circRNA) that can sequester the Mbl protein (*39*, *40*). To assess whether *Dscam2* exon 10B selection is dependent on a specific alternative variant of Mbl, we overexpressed the complementary DNAs (cDNAs) of fly *mbl* isoforms [*mblA*, *mblB*, and *mblC*; (*29*)], as well as an isoform of the human *MBNL1* that lacks the linker region optimal for *CUG* repeat binding [*MBNL1*$_{35}$; (*41*)] with either *Act5c-Gal4* or *OK107-Gal4*. These constructs all have the tandem N-terminal CCCH motif that binds to the consensus YCGY motif (*29*) and lack the ability to produce *mbl* circRNA (*40*). In all cases, OE resulted in the misexpression of *Dscam2.10B* in α′β′ MBs (with the exception of *Act5C>mblC*, which resulted in lethality; Fig. 4, D and E). Using semiquantitative RT-PCR from the *Act5C>mbl* flies, we demonstrated that OE of *mbl* did not lead to exon 10 skipping and that it increased exon 10B selection by 8 to 24% (Fig. 4F), depending on the *mbl* isoform used. The inability of Mbl to completely inhibit exon 10A selection suggests that other factors or mechanisms may also contribute to cell-specific *Dscam2* isoform expression (see Discussion). These results suggest that Mbl protein isoforms are all capable of *Dscam2.10B* selection and independent of *mbl* circRNA. The ability of human MBNL1 to promote the selection of exon 10B suggests that the regulatory logic for *Dscam2* splicing is likely conserved in other mutually exclusive cassettes in higher organisms. Together, our results show that all *mbl* isoforms are sufficient to promote *Dscam2.10B* selection.

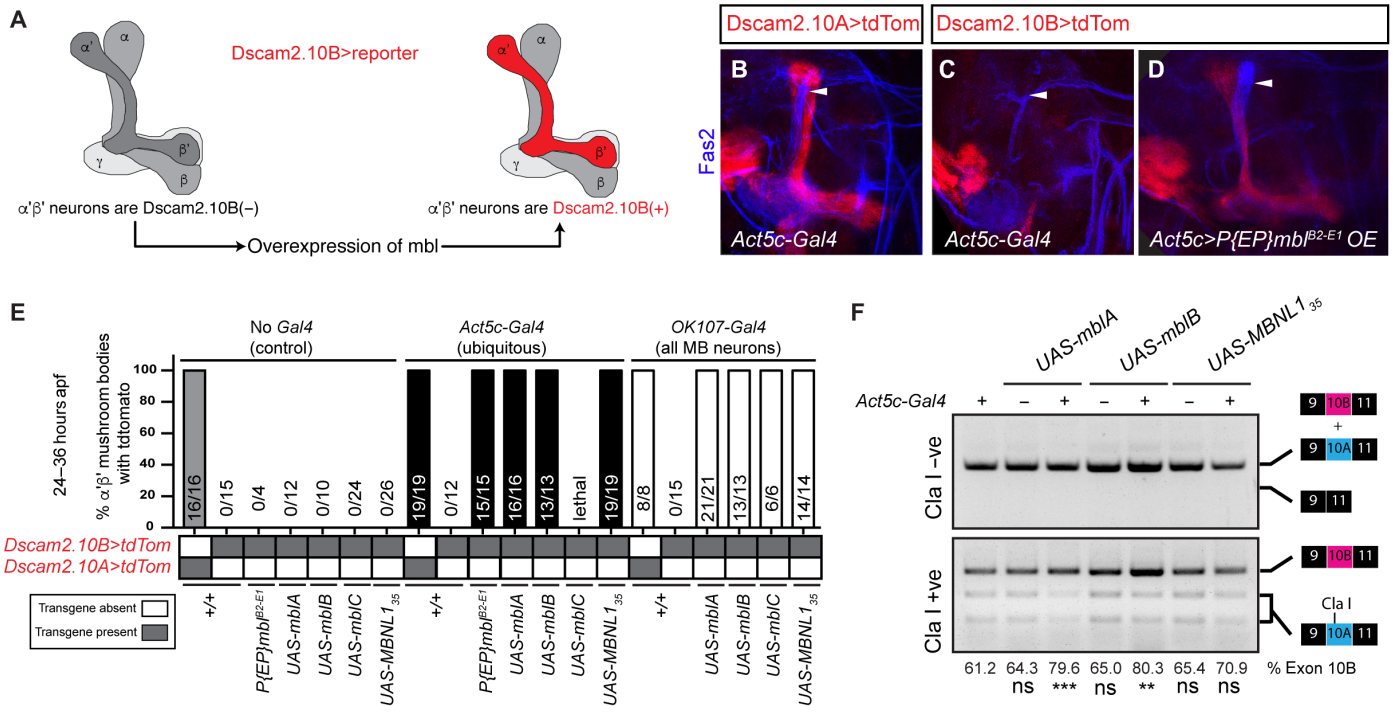

Fig. 4. Multiple *mbl* isoforms promote selection of *Dscam2* exon 10B. (**A**) Schematic showing that *mbl* is sufficient to drive *Dscam2.10B* selection in α′β′ neurons. (**B**) Control showing that *Dscam2.10A* (red) is expressed in α′β′ neurons at 24 hours apf. (**C**) *Dscam2.10B* is normally repressed in α′β′ neurons. (**D**) OE of *mbl* activates *Dscam2.10B* selection (red) in α′β′ neurons. (**E**) Quantification of *Dscam2.10* expression in α′β′ neurons at 24 to 36 hours apf with and without *mbl* OE. Control (No *Gal4*, gray bar), ubiquitous driver (*Act5c-Gal4*, black bars), and pan-MB neuron driver (*OK107-Gal4*, white bars). *Y* axis represents the number of tdTom-positive (+) α′β′ over the total, expressed as a percentage. Ratio of tdTom(+)/total is shown in each bar. (**F**) *Mbl* OE increases *Dscam2* exon 10B inclusion. Semiquantitative RT-PCR as in Fig. 1. Exon 10A–specific cleavage with restriction enzyme Cla I shows an increase in exon 10B inclusion in *mbl* OE animals, without exon 10 skipping. The percentage of exon 10B inclusion was calculated by dividing 10B by 10A+10B bands following electrophoresis and densitometry. The mean of exon 10B inclusion is shown at the bottom of each lane. ANOVA test with Tukey's multiple comparison test was used to compare the exon 10B inclusion. ns, $P > 0.05$; $^{**}P < 0.01$; $^{***}P < 0.001$.

Mbl regulates cell type–specific *Dscam2* alternative splicing in lamina neurons

To determine whether the regulatory logic of *Dscam2* alternative splicing is consistent in other cell types, we manipulated *mbl* expression in lamina neurons (L1 to L5). We first asked whether *mbl* LOF resulted in the derepression of *Dscam2.10A* in L1 neurons. To do this, we visualized *Dscam2* isoform expression in L1 to L5 using an intersectional strategy similar to Fig. 3 but with a different *FLP* source (*27G05-FLP*). We detected L1 and L4 neurons when using the *Dscam2.10B-Gal4* reporter in a wild-type background, but not L2, L3, or L5. L1 was also not detected when using the *Dscam2.10A-Gal4* reporter, where L2 to L5 cells were the primary neurons labeled (Fig. 5A). Consistent with our R cell results, derepression of *Dscam2.10A* was observed in L1 neurons in *mbl* transheterozygous animals ($mbl^{e127}/mbl^{MI00976}$) when compared to the corresponding heterozygous controls (mbl^{e127}/+ and $mbl^{MI00976}$/+; Fig. 5, A and B). We next asked whether ectopic OE of *mbl* would result in aberrant *Dscam2.10B* selection in L2, L3, and L5 neurons where it is usually repressed. For this experiment, the *Gal4/UAS* system was used to overexpress *mbl*, and the *LexA/LexAop* system was used to visualize *Dscam2* isoform expression. Using the same intersectional strategy, we found that *Dscam2-LexA* reporters showed similar patterns to the *Dscam2-Gal4* reporters (Fig. 5C). Pan-neuronal OE (*elav-Gal4*) of *mbl* caused the aberrant detection of *Dscam2.10B* in L2, L3, and L5 cells that normally select *Dscam2.10A* (Fig. 5, C and D). Together, our results show that Mbl regulates *Dscam2* cell type–specific alternative splicing. The simple presence or absence of *mbl* is sufficient to determine whether a cell expresses *Dscam2.10A* or *Dscam2.10B*.

Manipulation of *mbl* expression generates phenotypes observed in *Dscam2* single-isoform mutants

If Mbl regulates *Dscam2* alternative splicing, *mbl* LOF and OE animals should exhibit similar phenotypes to *Dscam2* isoform misexpression. Previously, we showed that flies expressing a single isoform of *Dscam2* exhibit a reduction in L1 axon arbor size as well as reduced dendritic width (*4*, *23*). These flies were generated using recombinase-mediated cassette exchange and express a single isoform in all *Dscam2*-positive cells (*4*). The reduction in axonal arbors and dendritic widths was proposed to be due to inappropriate interactions between cells that normally express different isoforms. Consistent with these previous studies, we observed a reduction in the area of L1 axon arbors (more prominent in m1 than in m5; Fig. 5, E, F, I, and J) and the width of dendritic arrays (Fig. 5, G, H, and K) in *mbl*

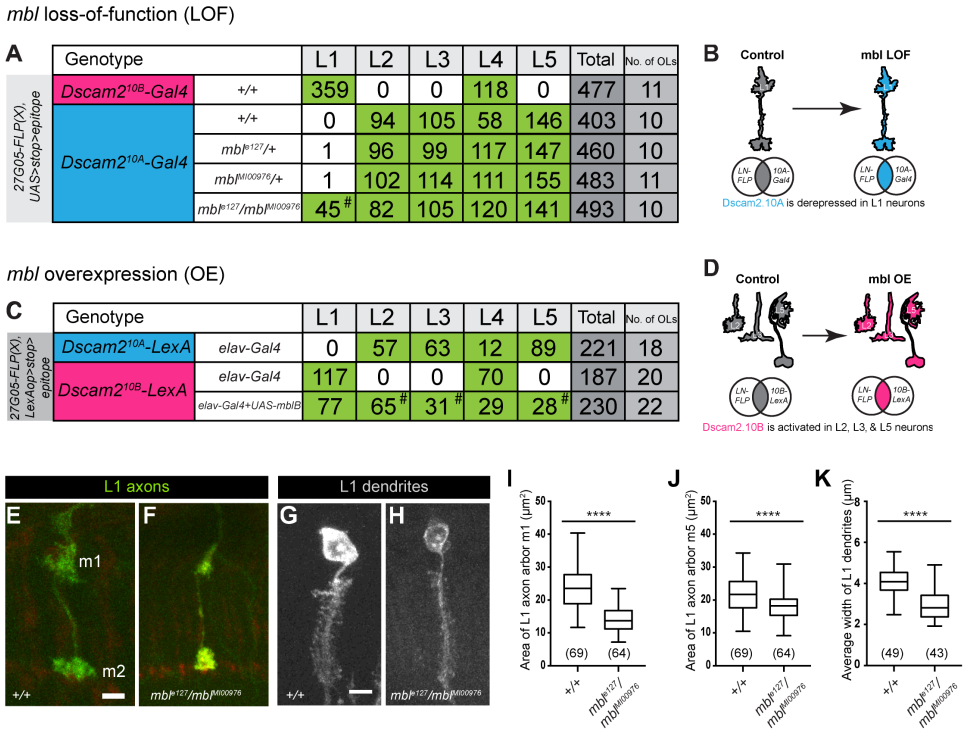

Fig. 5. Mbl regulates *Dscam2* cell type–specific alternative splicing in lamina neurons. (**A**) Quantification of lamina neurons L1 to L5 observed using the *Dscam2.10B-Gal4* (magenta) or *Dscam2.10A-Gal4* (blue) reporters with the intersectional strategy in *mbl* LOF animals. Green boxes represent a high number of labeled neurons. *Dscam2.10A* is derepressed in L1 neurons in an *mbl* LOF background ($mbl^{MI00976}/mbl^{e27}$, hashtag). (**B**) Schematic of *Dscam2.10A* derepression in *mbl* LOF L1 neurons. (**C**) Quantification of lamina neurons L1 to L5 observed using the *Dscam2.10A-LexA* (blue) or *Dscam2.10B-LexA* (magenta) reporters with the intersectional strategy in animals with pan-neuronal (*elav-Gal4*) expression of *mbl*. Green boxes represent high numbers of labeled neurons. *Dscam2.10B-LexA* was aberrantly detected in L2, L3, and L5 neurons overexpressing *mblB* (hashtag). (**D**) Schematic of aberrant *Dscam2.10B* selection in L2, L3, and L5 neurons overexpressing *mbl*. (**E** to **K**) L1 neurons in *mbl* LOF animals have reduced axon arbor area and dendritic array width when compared to controls. (E) Representative confocal image of a control L1 axon (green) with arbors at m1 and m5 layers. (F) Representative confocal image of an L1 axon from *mbl* LOF animals ($mbl^{MI00976}/mbl^{e27}$). (G) Representative confocal image of a control L1 dendritic array (gray). (H) Representative confocal image of an L1 dendritic array from *mbl* LOF animals ($mbl^{MI00976}/mbl^{e27}$). (I) Quantification of an L1 axon m1 arbor area (μm^2). (J) Quantification of an L1 axon m5 arbor area (μm^2). (K) Quantification of L1 dendritic width (μm). Tukey boxplot format: middle line, median; range bars, min and max; box, 25 to 75% quartiles; and each data point, single cartridge. Numbers in parentheses represent total numbers of L1 neurons quantified. Parametric *t* test was used to compare *mbl* LOF L1 axon arbor area with controls. Nonparametric *t* test was used to compare *mbl* LOF L1 dendritic width with controls. ****$P < 0.0001$. Scale bars, 5 μm (E to H).

transheterozygous animals ($mbl^{e127}/mbl^{MI00976}$) when compared to controls. Finally, we observed a phenotype in MB neurons overexpressing *mbl*, where the β lobe neurons inappropriately crossed the midline (fig. S5, A to C). A similar phenotype was observed in *Dscam2A* single-isoform mutants. These data demonstrate that MB phenotypes generated in animals overexpressing *mbl* phenocopy *Dscam2* single-isoform mutants. While the origin of this nonautonomous phenotype is not known, it correlates with the misregulation of *Dscam2* alternative isoform expression.

DISCUSSION

In this study, we identify Mbl as a regulator of *Dscam2* alternative splicing. We demonstrate that removing *mbl* in an *mbl*-positive cell type results in a switch from *Dscam2.10B* to *Dscam2.10A* selection. Ectopic expression of a variety of Mbl protein isoforms in a normally *mbl*-negative neuronal cell type is sufficient to trigger the selection of *Dscam2.10B*. Consistent with this, transcriptional reporters demonstrate that *mbl* is expressed in a cell type–specific manner in multiple cell types, which tightly correlates with *Dscam2.10B*. Last, both *mbl* LOF and misexpression lead to phenotypes that are observed in flies that express a single *Dscam2* isoform.

Our data demonstrate that *mbl* is expressed in a cell-specific fashion. In the lamina of the fly visual system, L1 and L2 neurons are developmentally very similar in terms of both morphology and gene expression (*37*). The difference in *mbl* expression between these two cells is critical for their development because, when expression of this splicing factor is perturbed, both cells express the same isoform, and inappropriate Dscam2 interactions lead to phenotypes in their axons and dendrites. Although cell-specific *mbl* expression has been alluded to previously (*42*–*44*), our study demonstrates that *mbl* regulation of *Dscam2* alternative splicing has functional consequences. Mbl appears to be regulated at the transcriptional level because the enhancer-trap as well as splicing-trap reporters lack the components crucial for posttranscriptional regulation yet still exhibit cell type–specific expression (Fig. 3). This was unexpected as a recent study showed that *mbl* encodes numerous alternative isoforms that could be individually posttranscriptionally repressed by different microRNAs, thus bypassing the need for transcriptional control of the gene (*45*). It will be interesting to explore the in vivo expression patterns of other splicing factors in *Drosophila* to determine whether cell-specific expression of a subset of splicing factors is a common mechanism for regulating alternative splicing in the brain.

The expression pattern of *mbl* and its ability to simultaneously repress exon 10A and select exon 10B suggest that this RNA binding protein and its associated cofactors are sufficient to regulate cell type–specific splicing of *Dscam2*. *Dscam2.10A* could be the default exon selected when the Mbl complex is absent. In this way, cells that express *mbl* select *Dscam2.10B*. Consistent with this, ectopic expression of *mbl* in *mbl*-negative cells (L2, L3, L5, and α′β′ neurons) results in the aberrant selection of exon 10B. Our RT-PCR data, however, argue that *Dscam2* mutually exclusive alternative splicing may be more complicated than this model. Ubiquitous expression of *mbl* increased exon B inclusion modestly (up to 24%) as measured by RT-PCR (see Fig. 4F). One might expect a more pronounced shift to isoform B if Mbl were the only regulator/mechanism involved. Further studies, including screens for repressors of exon 10B, will be required to resolve this issue.

The L1 axon and dendrite phenotypes generated through the LOF and ectopic expression of *mbl*, respectively, demonstrate that this splicing factor regulates aspects of neurodevelopment through cell-specific expression of *Dscam2* isoforms. In the lamina, *mbl* expression in L1, and its absence in L2, permits these neurons to express distinct Dscam2 proteins that cannot recognize each other. Phenotypes arise in these neurons both when they are engineered to express the same isoform (*4*, *23*) and when *mbl* is misregulated (Fig. 5). These data strongly link the regulation of cell-specific *Dscam2* splicing with normal neuron development.

Mbl OE also generates a midline crossing phenotype in MB neurons that is similar to that observed in animals expressing a single isoform. This phenotype is complicated, however, by the observation that *Dscam2.10A*, but not *Dscam2.10B*, animals show a statistically significant increase in midline crossing compared to controls (fig. S4). This issue may have to do with innate differences between isoform A and isoform B that are not completely understood. It is possible that isoforms A and B are not identical in terms of signaling because of either differences in homophilic binding or differences in cofactors associated with specific isoforms. Consistent with this notion, we previously reported that *Dscam2.10A* single-isoform lines produce stronger phenotypes at photoreceptor synapses compared to *Dscam2.10B* (*23*).

How does Mbl repress *Dscam2.10A* and select *Dscam2.10B* at the level of pre-mRNA? The best-characterized alternative splicing events regulated by human MBNL1 are exon skipping or inclusion events. In general, an exon that contains MBNL1 binding sites upstream or within the coding sequence is subject to skipping, whereas downstream binding sites more often promote inclusion. The mechanisms used by fly Mbl to regulate splicing have not been characterized in detail, but given that human MBNL1 can rescue fly *mbl* lethality (*46*) and promote the endogenous expression of *Dscam2* exon 10B in MBs, presumably the mechanisms are conserved. A simple explanation for how Mbl regulates *Dscam2* mutually exclusive splicing would be that it binds upstream of exon 10A to repress exon inclusion and downstream of exon 10B to promote inclusion. Although there are many potential binding sites for Mbl upstream, downstream, and within the alternative exons, an obvious correlation between location and repression versus inclusion is not observed. In total, there are 63 potential Mbl binding sites (YCGY) within the 5-kb variable region of *Dscam2*. Identification of the sequences required for regulation by Mbl will therefore require extensive mapping and, ultimately, validation using a technique like CLIP (cross-linking followed by immunoprecipitation) (*47*) or TRIBE (targets of RNA binding proteins identified by editing) (*48*).

Together, our results demonstrate that the simple presence or absence of a splicing factor can affect neurodevelopment through the cell-specific selection of distinct isoforms of a cell surface protein. We provide compelling genetic evidence of how Mbl regulates the alternative splicing of *Dscam2*, and this regulatory logic is likely to extend to cover the splicing events of many other genes crucial for neurodevelopment. Developmental analysis of *mbl* expression in the cells studied here suggests that it turns on after neurons have obtained their identity (similar to *Dscam2*) and is therefore well suited for regulating processes such as axon guidance and synapse specification. Identifying these splicing events may provide clues as to how the brain can diversify and regulate its repertoire of proteins to promote neural connectivity.

MATERIALS AND METHODS

Fly strains

The following fly strains were used: *Dscam2.10A-LexA* and *Dscam2.10B-LexA* (*24*), *UAS-Dcr2* and *UAS-mbl-RNAi*^{VDRC28732}, *LexAop-myr-tdTomato* (attP2), *UAS-Srp54-RNAi*$^{TRiP.HMS03941}$, *CadN-RNAi*$^{TRiP.HMS02380}$ and *UAS-mbl-RNAi*$^{TRiP.JF03264}$, *UAS-mCD8-GFP* (*32*), *FRT42D*, *mbl*^{e127} and *mbl*^{e27} (*29*), *mbl*^{MI00976} and *mbl*^{MI04093}, *Df(2R)BSC154*, *Df(2R)Exel6066*, *ey-FLP* (Chr.1), *GMR-myr-GFP*, *mbl*^{NP0420}*-Gal4* and *mbl*^{NP1161}*-Gal4*, *mbl*^{k01212}*-LacZ*, *mbl*^{MiMIC00139}*-Gal4* (H. Bellen Lab), *Dac-FLP* (Chr.3) (*21*), *UAS>stop>myr::smGdP-V5-THS-UAS>stop>myr::smGdP-cMyc* (attP5) (*36*), *Dscam2.10A-Gal4* and *Dscam2.10B-Gal4* (*4*), *Act5C-Gal4* (Chr.3, from Y. Hiromi), *OK107-Gal4*, *UAS-mblA*, *UAS-mblB* and *UAS-mblC* (D. Yamamoto Lab), *P{EP}mbl*$^{B2-E1}$, *UAS-mblA-FLAG*, and *UAS-MBNL1*$_{35}$ (*41*).

RNAi screening

The RNAi screen line was generated as follows: *GMR-Gal4* was recombined with *GMR-GFP* on the second chromosome. *Dscam2.10A-LexA* was recombined with *LexAop-myr-tdTomato* on the third chromosome. These flies were crossed together with *UAS-Dcr-2* (X) to make a stable RNAi screen stock. *UAS-RNAi* lines were obtained from Bloomington Drosophila Stock Center and Vienna Drosophila Resource Center. Lethal *UAS-RNAi* stocks were placed over balancers with developmentally selectable markers. Virgin females were collected from the RNAi screen stock, crossed to *UAS-RNAi* males, and reared at 25°C. Wandering third-instar larvae were dissected and fixed. We tested between one and three independent RNAi lines per gene. In total, we imaged ~2300 third-instar optic lobes without antibodies using confocal microscopy at 63×. RNAi lines tested are listed in table S1.

Semiquantitative and quantitative RT-PCR

Total RNA was isolated using TRIzol (Ambion) following the manufacturer's protocol. Reverse transcription was performed on each RNA sample with random primer mix [semiquantitative; New England Biolabs (NEB)] or Oligo-dT (qRT-PCR; NEB) using 200 U of Moloney murine leukemia virus reverse transcriptase (NEB) and 1 μg of RNA in a 20-μl reaction at 42°C for 1 hour. PCRs were set up with specific primers to analyze alternative splicing of various regions of *Dscam2*. Where possible, semiquantitative PCR was performed to generate multiple isoforms in a single reaction, and relative levels were compared by electrophoresis followed by densitometry. For qRT-PCR, 1 μl of cDNA was added to a Luna Universal SYBR-Green qPCR Master Mix kit (NEB). Samples were added into a 200-μl 96-well plate and read on a QuantStudio TM 6 Flex Real-Time PCR machine. R_q values were calculated in Excel (Microsoft).

Immunohistochemistry

Immunostaining was conducted as previously described (*4*). Antibody dilutions used were as follows: mouse mAb24B10 [1:20; Developmental Studies Hybridoma Bank (DSHB)], mouse anti-Repo (1:20; DSHB), mouse anti-Dacshund (1:20; DSHB), mouse anti-Fas2 (1:20; DSHB) rat anti–embryonic lethal abnormal vision (ELAV) (1:200), V5-tag: DyLight anti-mouse 550 (1:500; AbD Serotec), V5-tag:DyLight anti-mouse 405 (1:200; AbD Serotec), myc-tag:DyLight anti-mouse 549 (1:200; AbD Serotec), phalloidin/Alexa Fluor 568 (1:200; Molecular Probes), DyLight anti-mouse 647 (1:2000; Jackson Laboratory), and DyLight Cy3 anti-rat (1:2000; Jackson Laboratory).

Image acquisition

Imaging was performed at the School of Biomedical Sciences Imaging Facility. Images were taken on a Leica SP8 laser scanning confocal system with a 63× glycerol NA (numerical aperture) 1.3.

Fly genotypes

Specific genotypes can be found in the Supplementary Materials.

SUPPLEMENTARY MATERIALS

Supplementary material for this article is available at http://advances.sciencemag.org/cgi/content/full/5/1/eaav1678/DC1

Supplementary Materials

Fig. S1. *Mbl* LOF results in aberrant *Dscam2.10A* reporter expression in eye mosaic clones.

Fig. S2. *Mbl* LOF is associated with increased *Dscam2.10A* inclusion without affecting other *Dscam2* splicing events.

Fig. S3. *Mbl* is expressed in R cells, neurons, and glia.

Fig. S4. *Mbl* expression is cell type specific and correlates with *Dscam2.10B*.

Fig. S5. Neurons overexpressing *mbl* phenocopy *Dscam2* single-isoform mutants.

Table S1. List of tested RNAi lines that did not derepress *Dscam2.10A* in R cells.

REFERENCES AND NOTES

1. Q. Pan, O. Shai, L. J. Lee, B. J. Frey, B. J. Blencowe, Deep surveying of alternative splicing complexity in the human transcriptome by high-throughput sequencing. *Nat. Genet.* **40**, 1413–1415 (2008).
2. E. T. Wang, R. Sandberg, S. Luo, I. Khrebtukova, L. Zhang, C. Mayr, S. F. Kingsmore, G. P. Schroth, C. B. Burge, Alternative isoform regulation in human tissue transcriptomes. *Nature* **456**, 470–476 (2008).
3. T. Iijima, Y. Iijima, H. Witte, P. Scheiffele, Neuronal cell type-specific alternative splicing is regulated by the KH domain protein SLM1. *J. Cell Biol.* **204**, 331–342 (2014).
4. G. J.-e. Lah, J. S. Li, S. S. Millard, Cell-specific alternative splicing of *Drosophila Dscam2* is crucial for proper neuronal wiring. *Neuron* **83**, 1376–1388 (2014).
5. M. Tomioka, Y. Naito, H. Kuroyanagi, Y. Iino, Splicing factors control *C. elegans* behavioural learning in a single neuron by producing DAF-2c receptor. *Nat. Commun.* **7**, 11645 (2016).
6. T. J. Bell, C. Thaler, A. J. Castiglioni, T. D. Helton, D. Lipscombe, Cell-specific alternative splicing increases calcium channel current density in the pain pathway. *Neuron* **41**, 127–138 (2004).
7. A. D. Norris, S. Gao, M. L. Norris, D. Ray, A. K. Ramani, A. G. Fraser, Q. Morris, T. R. Hughes, M. Zhen, J. A. Calarco, A pair of RNA-binding proteins controls networks of splicing events contributing to specialization of neural cell types. *Mol. Cell* **54**, 946–959 (2014).
8. D. Schreiner, T.-M. Nguyen, G. Russo, S. Heber, A. Patrignani, E. Ahrné, P. Scheiffele, Targeted combinatorial alternative splicing generates brain region-specific repertoires of neurexins. *Neuron* **84**, 386–398 (2014).
9. T. W. Nilsen, B. R. Graveley, Expansion of the eukaryotic proteome by alternative splicing. *Nature* **463**, 457–463 (2010).
10. M. Blanchette, R. E. Green, S. MacArthur, A. N. Brooks, S. E. Brenner, M. B. Eisen, D. C. Rio, Genome-wide analysis of alternative pre-mRNA splicing and RNA-binding specificities of the *Drosophila* hnRNP A/B family members. *Mol. Cell* **33**, 438–449 (2009).
11. V. Markovtsov, J. M. Nikolic, J. A. Goldman, C. W. Turck, M.-Y. Chou, D. L. Black, Cooperative assembly of an hnRNP complex induced by a tissue-specific homolog of polypyrimidine tract binding protein. *Mol. Cell. Biol.* **20**, 7463–7479 (2000).
12. J. G. Underwood, P. L. Boutz, J. D. Dougherty, P. Stoilov, D. L. Black, Homologues of the *Caenorhabditis elegans* Fox-1 protein are neuronal splicing regulators in mammals. *Mol. Cell. Biol.* **25**, 10005–10016 (2005).
13. C. C. Warzecha, T. K. Sato, B. Nabet, J. B. Hogenesch, R. P. Carstens, ESRP1 and ESRP2 are epithelial cell-type-specific regulators of FGFR2 splicing. *Mol. Cell* **33**, 591–601 (2009).
14. H. Kuroyanagi, T. Kobayashi, S. Mitani, M. Hagiwara, Transgenic alternative-splicing reporters reveal tissue-specific expression profiles and regulation mechanisms in vivo. *Nat. Methods* **3**, 909–915 (2006).
15. G. Ohno, M. Hagiwara, H. Kuroyanagi, STAR family RNA-binding protein ASD-2 regulates developmental switching of mutually exclusive alternative splicing in vivo. *Genes Dev.* **22**, 360–374 (2008).
16. J. A. Calarco, S. Superina, D. O'Hanlon, M. Gabut, B. Raj, Q. Pan, U. Skalska, L. Clarke, D. Gelinas, D. van der Kooy, M. Zhen, B. Ciruna, B. J. Blencowe, Regulation of vertebrate nervous system alternative splicing and development by an SR-related protein. *Cell* **138**, 898–910 (2009).
17. A. E. McKee, E. Minet, C. Stern, S. Riahi, C. D. Stiles, P. A. Silver, A genome-wide in situ hybridization map of RNA-binding proteins reveals anatomically restricted expression in the developing mouse brain. *BMC Dev. Biol.* **5**, 14 (2005).

18. Q. Wang, K. C. Abruzzi, M. Rosbash, D. C. Rio, Striking circadian neuron diversity and cycling of *Drosophila* alternative splicing. *eLife* **7**, e35618 (2018).
19. M. Funada, H. Hara, H. Sasagawa, Y. Kitagawa, T. Kadowaki, A honey bee Dscam family member, AbsCAM, is a brain-specific cell adhesion molecule with the neurite outgrowth activity which influences neuronal wiring during development. *Eur. J. Neurosci.* **25**, 168–180 (2007).
20. S. S. Millard, Z. Lu, S. L. Zipursky, I. A. Meinertzhagen, *Drosophila* dscam proteins regulate postsynaptic specificity at multiple-contact synapses. *Neuron* **67**, 761–768 (2010).
21. S. S. Millard, J. J. Flanagan, K. S. Pappu, W. Wu, S. L. Zipursky, Dscam2 mediates axonal tiling in the *Drosophila* visual system. *Nature* **447**, 720–724 (2007).
22. J. S. Li, G. J.-e. Shin, S. S. Millard, Neuronal cell-type-specific alternative splicing: A mechanism for specifying connections in the brain? *Neurogenesis* **2**, e1122699 (2015).
23. S. K. Kerwin, J. S. S. Li, P. G. Noakes, G. J.-e. Shin, S. S. Millard, Regulated alternative splicing of *Drosophila Dscam2* is necessary for attaining the appropriate number of photoreceptor synapses. *Genetics* **208**, 717–728 (2018).
24. W. Tadros, S. Xu, O. Akin, C. H. Yi, G. J.-e. Shin, S. S. Millard, S. L. Zipursky, Dscam proteins direct dendritic targeting through adhesion. *Neuron* **89**, 480–493 (2016).
25. A. H. Brand, N. Perrimon, Targeted gene expression as a means of altering cell fates and generating dominant phenotypes. *Development* **118**, 401–415 (1993).
26. K. Mondal, K. VijayRaghavan, R. Varadarajan, Design and utility of temperature-sensitive Gal4 mutants for conditional gene expression in Drosophila. *Fly* **1**, 282–286 (2007).
27. M. Pascual, M. Vicente, L. Monferrer, R. Artero, The Muscleblind family of proteins: An emerging class of regulators of developmentally programmed alternative splicing. *Differentiation* **74**, 65–80 (2006).
28. A. Kania, A. Salzberg, M. Bhat, D. D'Evelyn, Y. He, I. Kiss, H. J. Bellen, P-element mutations affecting embryonic peripheral nervous system development in Drosophila melanogaster. *Genetics* **139**, 1663–1678 (1995).
29. G. Begemann, N. Paricio, R. Artero, I. Kiss, M. Pérez-Alonso, M. Mlodzik, *muscleblind*, a gene required for photoreceptor differentiation in *Drosophila*, encodes novel nuclear Cys_3His-type zinc-finger-containing proteins. *Development* **124**, 4321–4331 (1997).
30. U. Irion, *Drosophila muscleblind* codes for proteins with one and two tandem zinc finger motifs. *PLOS ONE* **7**, e34248 (2012).
31. R. Artero, A. Prokop, N. Paricio, G. Begemann, I. Pueyo, M. Mlodzik, M. Perez-Alonso, M. K. Baylies, The *muscleblind* gene participates in the organization of Z-bands and epidermal attachments of *Drosophila* muscles and is regulated by *Dmef2*. *Dev. Biol.* **195**, 131–143 (1998).
32. T. Lee, L. Luo, Mosaic analysis with a repressible cell marker for studies of gene function in neuronal morphogenesis. *Neuron* **22**, 451–461 (1999).
33. J. Brouwer, D. Nagelkerke, P. den Heijer, J. H. Ruiter, H. Mulder, M. J. S. Begemann, K. I. Lie, Analysis of atrial sensed far-field ventricular signals: A reassessment. *Pacing Clin. Electrophysiol.* **20**, 916–922 (1997).
34. F. Diao, H. Ironfield, H. Luan, F. Diao, W. C. Shropshire, J. Ewer, E. Marr, C. J. Potter, M. Landgraf, B. H. White, Plug-and-play genetic access to *Drosophila* cell types using exchangeable exon cassettes. *Cell Rep.* **10**, 1410–1421 (2015).
35. A. Bargiela, B. Llamusi, E. Cerro-Herreros, R. Artero, Two enhancers control transcription of *Drosophila muscleblind* in the embryonic somatic musculature and in the central nervous system. *PLOS ONE* **9**, e93125 (2014).
36. A. Nern, B. D. Pfeiffer, G. M. Rubin, Optimized tools for multicolor stochastic labeling reveal diverse stereotyped cell arrangements in the fly visual system. *Proc. Natl. Acad. Sci. U.S.A.* **112**, E2967–E2976 (2015).
37. L. Tan, K. X. Zhang, M. Y. Pecot, S. Nagarkar-Jaiswal, P.-T. Lee, S. Y. Takemura, J. M. McEwen, A. Nern, S. Xu, W. Tadros, Z. Chen, K. Zinn, H. J. Bellen, M. Morey, S. L. Zipursky, Ig superfamily ligand and receptor pairs expressed in synaptic partners in *Drosophila*. *Cell* **163**, 1756–1769 (2015).
38. M. Vicente, L. Monferrer, M. G. Poulos, J. Houseley, D. G. Monckton, K. M. C. O'Dell, M. S. Swanson, R. D. Artero, Muscleblind isoforms are functionally distinct and regulate α-*actinin* splicing. *Differentiation* **75**, 427–440 (2007).
39. J. M. Houseley, Z. Garcia-Casado, M. Pascual, N. Paricio, K. M. C. O'Dell, D. G. Monckton, R. D. Artero, Noncanonical RNAs from transcripts of the *Drosophila muscleblind* gene. *J. Hered.* **97**, 253–260 (2006).
40. R. Ashwal-Fluss, M. Meyer, N. R. Pamudurti, A. Ivanov, O. Bartok, M. Hanan, N. Evantal, S. Memczak, N. Rajewsky, S. Kadener, circRNA biogenesis competes with pre-mRNA splicing. *Mol. Cell* **56**, 55–66 (2014).
41. L. B. Li, Z. Yu, X. Teng, N. M. Bonini, RNA toxicity is a component of ataxin-3 degeneration in *Drosophila*. *Nature* **453**, 1107–1111 (2008).
42. A. D. Norris, X. Gracida, J. A. Calarco, CRISPR-mediated genetic interaction profiling identifies RNA binding proteins controlling metazoan fitness. *eLife* **6**, e28129 (2017).
43. L. E. Machuca-Tzili, S. Buxton, A. Thorpe, C. M. Timson, P. Wigmore, P. K. Luther, J. D. Brook, Zebrafish deficient for Muscleblind-like 2 exhibit features of myotonic dystrophy. *Dis. Model. Mech.* **4**, 381–392 (2011).
44. H. Huang, K. J. Wahlin, M. McNally, N. D. Irving, R. Adler, Developmental regulation of muscleblind-like (MBNL) gene expression in the chicken embryo retina. *Dev. Dyn.* **237**, 286–296 (2008).
45. E. Cerro-Herreros, J. M. Fernandez-Costa, M. Sabater-Arcis, B. Llamusi, R. Artero, Derepressing *muscleblind* expression by miRNA sponges ameliorates myotonic dystrophy-like phenotypes in *Drosophila*. *Sci. Rep.* **6**, 36230 (2016).
46. L. Monferrer, R. Artero, An interspecific functional complementation test in *Drosophila* for introductory genetics laboratory courses. *J. Hered.* **97**, 67–73 (2006).
47. J. Ule, K. B. Jensen, M. Ruggiu, A. Mele, A. Ule, R. B. Darnell, CLIP identifies Nova-regulated RNA networks in the brain. *Science* **302**, 1212–1215 (2003).
48. A. C. McMahon, R. Rahman, H. Jin, J. L. Shen, A. Fieldsend, W. Luo, M. Rosbash, TRIBE: Hijacking an RNA-editing enzyme to identify cell-specific targets of RNA-binding proteins. *Cell* **165**, 742–753 (2016).

Acknowledgments: We thank W. Tadros, Y. Chen, L. Zipursky, G. Neely, L. O'Keefe, N. Bonini, A. Nern, and Bloomington Drosophila Stock Center for sharing fly stocks. We thank the Daisuke Yamamoto Lab for constructing the *UAS-mbl* lines deposited and maintained at the Kyoto Stock Center. We thank S. Walters for technical assistance on the Leica confocal microscopy. We note that G. Shin initially observed *Dscam2* isoform expression in the adult MBs. We thank K. Mutemi for thorough characterization of *Dscam2* isoform expression in MBs during development and all midline crossing defects in *Dscam2* single-isoform mutant animals. We thank W. J. Tan for the heroic feat of triple balancing *OK107-Gal4*. We also thank members of the Millard, Pecot, Hilliard, and van Swinderen laboratories for their feedback. The RNAi screen was inspired by the works of H. Kuroyanagi. **Funding:** This work was supported by the National Health and Medical Research Council of Australia (NHMRC grant APP1021006). J.S.S.L. was supported by the Australia Postgraduate Award (Research Training Scheme) from the Australian Federal Government and the Lavidis grant in aid. **Author contributions:** J.S.S.L. designed and performed all experiments. S.S.M. supervised the project. J.S.S.L. and S.S.M. wrote the manuscript. **Competing interests:** The authors declare that they have no competing interests. **Data and materials availability:** All data needed to evaluate the conclusions in the paper are present in the paper and/or the Supplementary Materials. Additional data related to this paper may be requested from the authors.

Submitted 22 August 2018
Accepted 4 December 2018
Published 16 January 2019
10.1126/sciadv.aav1678

Citation: J. S. S. Li, S. Sean Millard, Deterministic splicing of *Dscam2* is regulated by Muscleblind. *Sci. Adv.* **5**, eaav1678 (2019).